AIAA 99–3612

Energy Addition for Shockwave Control

Jonathan Poggie
US Air Force Research Laboratory
Wright-Patterson AFB, OH 45433-7521

30th Plasmadynamics and Lasers Conference
28 June-1 July, 1999/Norfolk, VA

Energy Addition for Shockwave Control

Jonathan Poggie*
US Air Force Research Laboratory
Wright-Patterson AFB, OH 45433-7521

An analytical and computational study was carried out to assess the relative importance of thermal effects in the experiments of Ganguly *et al.* (Physics Letters A, Vol. 230, 1997, pp. 218-222; Physics Letters A, 1999, to appear) on shock propagation in a glow discharge. Since measurements of the temperature field were not available, an analytical heating model was developed to relate the temperature field in the ionized gas to the discharge current. The temperatures predicted by the thermal model were used as initial conditions for one-dimensional and axisymmetric inviscid-flow models of shock propagation. The combination of the heating and flow models predicted shock speed as a function of the discharge current. For reasonable estimates of the input parameters in the gas heating model, it was possible to obtain an excellent fit of the shock speeds predicted by the model to the experimental data. The axisymmetric model predicted the double-peak in the photodetector signal that was observed in the experiments. Given the importance of thermal effects, future experiments must map the temperature field in detail in order to demonstrate that electromagnetic effects have a significant influence on shock propagation in a weakly-ionized plasma.

Nomenclature

Bi	Biot number, hr_3/k_s
C_p	constant pressure specific heat
D	tube outside diameter, $2r_3$
E	electric field
g	acceleration due to gravity
h	space-mean heat transfer coefficient
I	electric current
j	current density
k	thermal conductivity
k_B	Boltzmann constant
N	number density of neutral particles
Nu	Nusselt number, hD/k
Pr	Prandtl number, ν/α
q,Q	heat source parameters
Ra	Rayleigh number, $g\beta(T_w - T_\infty)D^3/\nu\alpha$
r,θ,z	cylindrical coordinates
t	time
T	temperature
V	fluid velocity
W	shock speed
x,y,z	Cartesian coordinates
α	thermal diffusivity, $k/\rho C_p$
β	thermal expansion coefficient
γ	specific heat ratio
δ	boundary layer thickness
η	fraction of power converted to heat
Θ	nondimensional temperature
μ	dynamic viscosity
ν	kinematic viscosity, μ/ρ
ρ	density

Subscripts

1-3	interfaces in thermal model
1-5	regions in 1D model
∞	uniform ambient conditions
c	undisturbed contact surface
g	gas
h	heat source
I	incident wave
s	solid
T	transmitted wave
w	wall

Superscripts

$*$	nondimensional variable

Introduction

Recent experimental research on the effects of introducing weak, nonequilibrium ionization upstream of a shock has revived interest in electromagnetic flow control for hypersonic air vehicles. For upstream fractional ionizations on the order of 10^{-8} to 10^{-6}, experiments have demonstrated changes in the speed, strength, and structure of shocks. In particular, reductions in heat transfer and drag have been claimed, based on the results of tests on wind tunnel models. A number of detailed bibliographies on this research are available.[1–5]

Interest has been motivated in part by the experiments of Klimov *et al.*,[6] in which a shock was generated with an electrical discharge and propagated down a tube through an ionized region. An increase in the speed and a decrease in the strength of the shock were observed with the presence of weak ionization upstream. Ganguly *et al.* have recently replicated and

*Research Aerospace Engineer, Air Vehicles Directorate, AFRL/VAAC, 2210 Eighth Street. Senior Member AIAA.

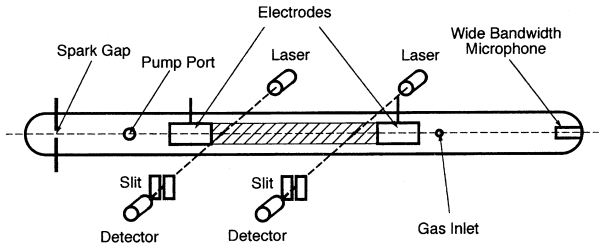

Fig. 1 Schematic diagram of experiments in glow discharge tube. From Ganguly *et al.*,[7] used with permission.

extended this work in two well-documented sets of experiments,[7,8] which will be the focus of the present paper. A schematic diagram of the apparatus for the first set of experiments[7] is shown in Fig. 1. The tests were carried out in a 50 mm diameter Pyrex tube, which was roughly 1 m long and was filled with argon gas. The pressure was fixed at about 4.0 kPa (30 torr) using a regulated purge flow. A shock was generated at the spark gap (left side of diagram, 272 mm from the start of the glow discharge) with an energy release of about 100 J. Downstream of the spark gap, a pair of 30 mm diameter cylindrical electrodes, separated by 300 mm, were used to generate a longitudinal plasma, with the cathode on the left in the diagram. The discharge was operated at constant current in the range 0 mA to 140 mA using a 10 kV, 300 mA direct current power supply. The arrival of the shock pulse was recorded using a laser deflection technique at two stations located 302 mm and 422 mm from the spark gap in the positive column of the glow discharge.

For the second set of experiments,[8] the working fluid was nitrogen and the experimental apparatus was slightly modified. In this case, the electrodes were mounted flush with the wall of the tube. The diameter of both the cylindrical electrodes and the tube was 30 mm, and the electrodes were separated by 200 mm. Laser deflection measurements were made at two pairs of stations, with each pair separated by 25.9 mm. Data were reported for pressures of 2.0 kPa (15 torr) and 2.7 kPa (20 torr).

Recent papers have addressed the possible physical mechanisms for the results obtained in the first set of spark-tube experiments.[3,5,9–12] Due to the low fractional ionization in the experiments, these studies have concluded that conventional mechanisms involving exothermic reactions and electromagnetic effects are not responsible for the experimental observations, but that thermal effects may be significant.

Possibly the first detailed study of thermal effects in the interaction of a shock with a glow discharge was carried out by Voinovich *et al.*,[13] who (for a different experiment in a conventional shock tube) successfully predicted shock velocities using measured temperature profiles as input to inviscid-flow theory and computations. More recently, Bailey and Hilbun[3,9] carried out a detailed analysis of thermal effects in the experiment of Ganguly *et al.*,[7] including a source/diffusion model for heating in the discharge and a two-dimensional (planar symmetry) inviscid-flow computation. Bailey and Hilbun obtained fairly good agreement between theory and experiment, although the test conditions provided to them are now believed to be incorrect (B. Ganguly, personal communication). Other recent computational studies have considered shock propagation through an assumed temperature profile, also employing a two-dimensional flow model with planar symmetry.[10,11]

Several objections to the previous computations of the spark-tube experiment can be raised. Unless a gas heating model is employed, it is not possible to make a quantitative comparison between the computations and the experimental data. Only Bailey and Hilbun make such a comparison; the other studies assume a temperature profile and make qualitative comparisons. Further, an axisymmetric computation is more appropriate to the experimental geometry than a computation with planar symmetry. Continuity considerations (the three-dimensional relieving effect[14]) suggest that less shock curvature should be present with axial symmetry.

The present study was undertaken to address these concerns. An analytical heating model was developed to relate the temperature field in the ionized gas to the discharge current. The predicted temperatures were used in a one-dimensional, analytical model and in an axisymmetric, inviscid-flow computation. The predictions of the models were then compared to the experimental data.

Heating Model

An analytical model was developed to predict the temperature field in the glow discharge experiments as a function of the applied current. A conceptual diagram is given in Fig. 2b, which is supposed to represent a cross-section of the glow discharge. The region $0 \le r \le r_2$ represents the gas, and the solid wall of the tube lies in the region $r_2 \le r \le r_3$. The gas-filled region is assumed to consist of two parts: the first ($0 \le r \le r_1$) is heated by a uniform source term representing Joule heating from the discharge current, and the second ($r_1 \le r \le r_2$) is unheated gas. For the present work, we take $r_1 = 15$ mm, $r_2 = 25$ mm, and $r_3 = 28$ mm to model the first experimental configuration and $r_1 = r_2 = 15$ mm and $r_3 = 18$ mm to model the second.

We assume that there is no gas flow inside tube before the passage of the shock, and solve a one-dimensional heat conduction equation in cylindrical coordinates:

$$\frac{1}{r}\frac{d}{dr}\left(r\frac{dT}{dr}\right) + q = 0 \qquad (1)$$

The source term is $q = Q/k_g$ in the inner layer ($0 \le r \le r_1$), and zero elsewhere.

The Joule heating term is given by $Q = \eta j E$. Here we take representative average values of these quantities: $j \approx I/\pi r_1^2$ and $E = (E/N)p/k_B T$, where E/N is assumed to be constant across the tube cross-section and independent of the discharge current. The source term is evaluated at the average temperature of the source region, T_h, given by Eq. (8), below.

Rough values for E/N are 1×10^{-21} V-m^2 (1 Td) for the first set of tests in argon and 3×10^{-20} V-m^2 (30 Td) for the second set in nitrogen (B. Ganguly, personal communication). Numerical solutions of the Boltzmann Equation[3] indicate that $\eta \approx 1$ for $E/N \approx 10^{-21}$ V-m^2 in argon. For the test conditions in nitrogen, most of the input energy should be transferred into vibrational modes,[15] so η will be relatively small. A detailed calculation of this parameter was beyond the scope of this paper; a value of $\eta = 0.2$ used with $E/N = 3 \times 10^{-20}$ V-m^2 gave a good fit of the model to the experimental data for nitrogen (see below).

The gas and the solid wall are assumed to have different, but constant, thermal conductivities. The thermal conductivities k_g and k_s were evaluated at the temperature, averaged over the circular cross-section, of the gas and solid from Eqs. (6) and (7). The thermal conductivity of each gas was evaluated using a curve fit of the Sutherland formula.[16] The thermal conductivity of the solid Pyrex was found by linear interpolation between published experimental values.[17]

A symmetry boundary condition is imposed at the centerline:

$$\left.\frac{dT}{dr}\right|_{r=0} = 0 \tag{2}$$

and a simple convection model is imposed at the outer boundary:

$$-k\left.\frac{dT}{dr}\right|_{r=r_3} = h\left[T(r_3) - T_\infty\right] \tag{3}$$

The heat transfer coefficient, h, is obtained from a semi-empirical equation for heat transfer (averaged over the surface) due to free convection over a horizontal, isothermal cylinder.[18]

$$\mathrm{Nu}^{1/2} = 0.60 + 0.387\left(\frac{\mathrm{Ra}}{\left[1 + (0.559/\mathrm{Pr})^{9/16}\right]^{16/9}}\right)^{1/6} \tag{4}$$

This equation is valid for $10^{-5} \le \mathrm{Ra} \le 10^{12}$, and over a wide range of Prandtl numbers. The transport coefficients in the Nusselt, Rayleigh, and Prandtl numbers are evaluated for room temperature air, and the wall temperature is the computed surface temperature, $T(r_3)$.

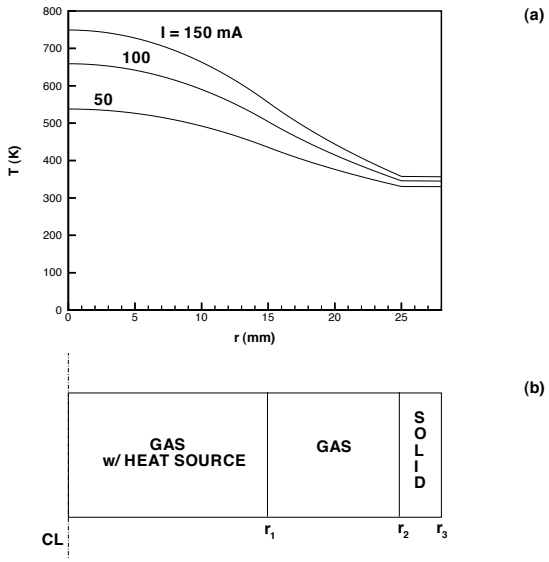

Fig. 2 Analytical heating model. (a) Temperature profiles (argon, 4 kPa). (b) Diagram.

Equation (1) is solved in each of the three regions, and the overall solution is obtained by matching the temperature and the heat flux at the interfaces between the regions. The solution has a parabolic form in the heated layer, and a logarithmic form elsewhere:

$$\frac{T(r) - T_\infty}{Qr_1^2/2k_g} = \begin{cases} \frac{1}{2}(1 - \frac{r^2}{r_1^2}) + \Theta_1 & 0 \le r \le r_1 \\ \ln\frac{r_2}{r} + \Theta_2 & r_1 \le r \le r_2 \\ \frac{k_g}{k_s}(\ln\frac{r_3}{r} + \frac{1}{\mathrm{Bi}}) & r_2 \le r \le r_3 \end{cases} \tag{5}$$

where $\Theta_2 = k_g/k_s[\ln(r_3/r_2) + 1/\mathrm{Bi}]$ and $\Theta_1 = \ln(r_2/r_1) + \Theta_2$. Average temperatures of the gas region, solid region, and source region, respectively, are found by integrating over annular regions of the domain:

$$\frac{T_g - T_\infty}{Qr_1^2/2k_g} = \frac{1}{2} - \frac{1}{4}\frac{r_1^2}{r_2^2} + \Theta_2 \tag{6}$$

$$\frac{T_s - T_\infty}{Qr_1^2/2k_g} = \frac{k_g}{k_s}\left[\frac{1}{2} - \frac{\ln(r_3/r_2)}{(r_3^2/r_2^2 - 1)} + \frac{1}{\mathrm{Bi}}\right] \tag{7}$$

$$\frac{T_h - T_\infty}{Qr_1^2/2k_g} = \frac{1}{4} + \ln\frac{r_2}{r_1} + \Theta_2 \tag{8}$$

Figure 2a shows example temperature profiles for three values of the discharge current for the case of 4 kPa argon. (Qualitatively similar results are obtained for nitrogen.) An iterative scheme was used to allow for the variation of the transport properties and the source term with temperature. The scale of the abscissa matches the schematic diagram in Fig. 2b.

Under steady-state conditions, the maximum temperature in the gas is set by the requirement of a sufficiently strong temperature gradient to conduct away the heat deposited by the source term. With its relatively low thermal conductivity, the gas supports large temperature gradients. In contrast, the relatively large

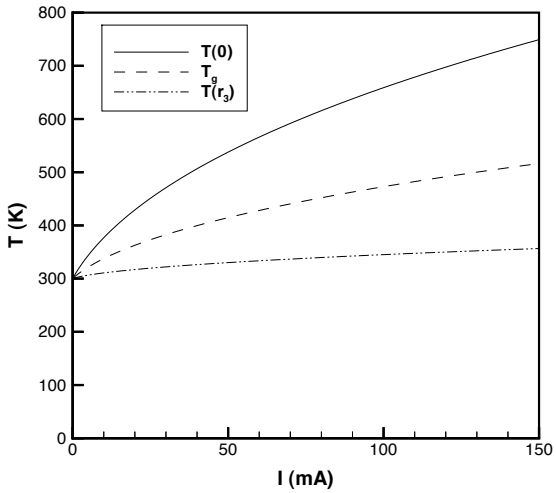

Fig. 3 Effect of discharge current on temperature (argon, 4 kPa).

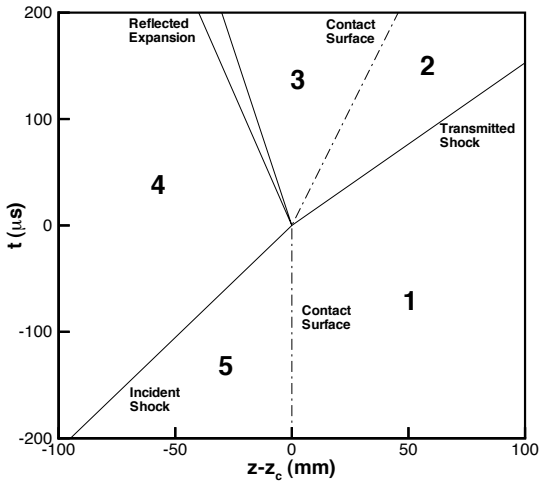

Fig. 4 Space-time diagram for normal reflection of a shock at a contact surface in argon ($M_I = 1.47$, $T_5 = 300$ K, $T_1 = 659$ K).

thermal conductivity of the Pyrex ($k_s \gg k_g$), and relatively weak convection at the outside wall (Bi $\sim 10^{-1}$), cause the temperature to remain essentially uniform throughout the Pyrex wall.

Figure 3 shows, for the same case, the centerline temperature, the average gas temperature, and the outside surface temperature as a function of the discharge current. Equations (5) and (6) indicate that these temperatures are linear in the source term Q; the curvature in the functions comes primarily from the variation of the source term and the gas thermal conductivity with temperature. As a result, the temperatures increase relatively slowly with current.

The most severe limitation of the present model is the assumption that no flow exists inside the tube before the passage of the shock. A calculation of the Rayleigh number based on the conditions inside the tube, and on the temperature difference between the centerline and the wall, gives a value on the order of Ra $\sim 10^5$. Considering the results reported in White[19] for free convection inside rectangular boxes as a rough comparison, a significant recirculating flow inside the tube is expected to exist in the experiments. Such a flow could significantly change the temperature field. A similar comment applies to the purge flow velocity profile, which was not quantified in the experiments.

1D Fluid Model

As a first model of the fluid dynamics, we will consider only the effect of thermal non-uniformity in the axial direction, replacing the radial temperature profile with a representative temperature. The interaction of the shock and the heated region will be modeled as a plane shock impinging at normal incidence on a plane contact surface.[20–23] The trailing expansion fan of the shock-pulse (which is generated by a spark in the experiments) will be ignored.

For the examples considered below, the working fluid was argon, the Mach number of the incident shock was taken to be $M_I = 1.47$ (determined from the experimental average shock speed between the two photodetector stations for the case with no plasma), and the solution was obtained for different values of the temperature of the heated region. The problem was solved by applying the secant method to finding the roots of the implicit equations of Ford and Glass.[23]

The problem is illustrated in the space-time diagram of Fig. 4. The numbers designate regions of uniform flow. For $t < 0$, the incident shock propagates to the right in the diagram toward a stationary contact surface which separates two still fluids at a given pressure (regions 1 and 5). Behind the shock lies a region (4) of uniform rightward flow at higher pressure. At $t = 0$, the shock hits the contact surface, generating transmitted and reflected waves. The transmitted wave is always a shock, but the reflected wave can be either a shock or a centered expansion fan, depending on the generalized acoustic impedance ratio of the contact surface. For the case under consideration here, where the gas on both sides of the contact surface is the same and the temperature is higher on the right, the reflected wave is an expansion. The initial and final characteristics of the expansion fan are shown in the figure, bounding a nonuniform region that separates regions 3 and 4. Two new regions (2 and 3) appear between the reflected and transmitted waves. The flow in these regions carries the contact surface to the right.

Figure 5 shows the effect of upstream temperature on the speed and strength of the transmitted shock. The point corresponding to $T_1 = 300$ K represents the case with no contact surface; here the incident

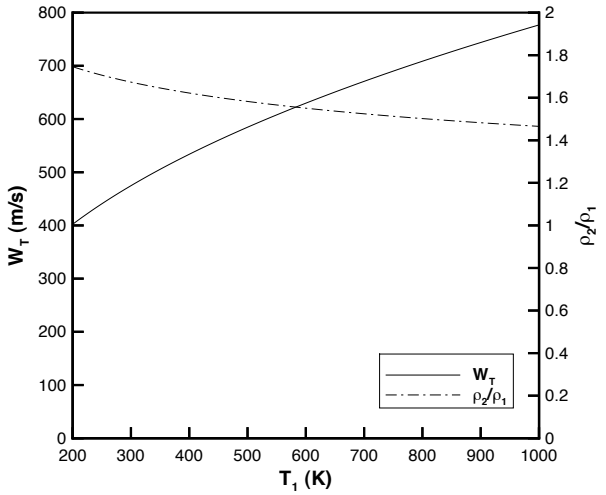

Fig. 5 Effect of upstream temperature on transmitted shock. (argon, $M_I = 1.47$, $T_5 = 300$ K).

shock propagates unimpeded to the right. For completeness, temperatures both lower (reflected shock) and higher (reflected expansion) are shown. The range where $T_1 > T_5$ is relevant to the current investigation, and shows the same qualitative behavior seen in the experiments: increased shock speed and decreased density ratio.

It is worth considering carefully the validity of the inviscid-flow assumption. Assuming that the boundary layer is laminar and unseparated, the boundary layer thickness downstream of the transmitted shock is given approximately by:[24–26]

$$\delta_{95\%} \approx 2.8\sqrt{\nu_2 x/(W_T - V_2)} \tag{9}$$

Evaluating this expression for 4 kPa argon at a distance one tube radius downstream of the shock ($x = r_2$) gives $\delta_{95\%} \approx 0.04 r_2$ for discharge currents in the range 0-150 mA, so the sidewall boundary layer is relatively thin. Bradley[27] suggests the following definition for a transition Reynolds number:

$$\mathrm{Re}_s = \frac{V_2^2 x}{(W_T - V_2)\nu_w} \tag{10}$$

with a critical value in the range 1×10^6 to 3×10^6. For the 4 kPa argon experiments, transition would not occur for over $100 r_2$ downstream of the shock. A relatively thin laminar boundary layer is expected to exist at the tube wall for the experiments in both nitrogen and argon.

2D Fluid Model

We now consider a two-dimensional, axisymmetric model for the flow. Computations were carried out using the three-dimensional code `fdl3d`, developed at the Air Force Research Laboratory. The equations

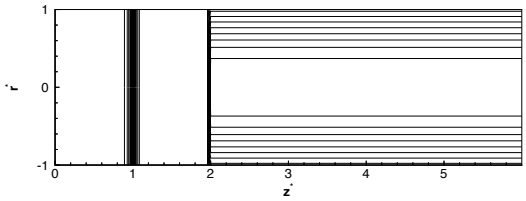

Fig. 6 Initial density field for $I = 100$ mA in 4 kPa argon. Contour interval $\Delta\rho^* = 0.05$.

for inviscid, compressible, perfect-gas flow were cast in strong conservation form and solved on a curvilinear coordinate system. Time marching was carried out using an explicit fourth-order Runge-Kutta scheme. The inviscid fluxes were discretized with Roe's flux-difference split scheme, implemented in a finite-difference formulation. For higher order accuracy, the state of the flow at each interface was obtained by extrapolating the vector of primitive variables with Van Leer's MUSCL algorithm. Van Leer's harmonic limiter was employed to stabilize the solution near shocks, reverting the method to formal first order accuracy in those regions. A flow- and mesh-based cutoff was applied to the two non-linear eigenvalues in each direction to enforce the entropy condition.

The problem was formulated in nondimensional variables. The inside tube radius was taken as the length scale, the density and velocity scales were taken to be the density and sound speed in Region 5 of Fig. 4, and the pressure scale was the density times the square of the sound speed. The computational domain was a wedge-shaped region ($0 \le \theta \le \pi/8$), six tube radii long ($0 \le z^* \le 6$), extending from the axis of symmetry to the inner wall of the tube ($0 \le r^* \le 1$). Uniform grid spacing was used along each coordinate, and the basic computations were carried out on a grid of $26 \times 5 \times 151$ points along the radial, circumferential, and axial directions, respectively. The time step was taken to be $\Delta t^* = 1 \times 10^{-3}$, in order to satisfy the CFL condition for the relatively small circumferential grid spacing near the axis of symmetry.

The initial conditions were taken to be a normal shock propagating to the right toward a contact surface, and are illustrated in Fig. 6. (In this figure, and those following, symmetry about $r^* = 0$ is used for clarity.) The expansion fan which is expected to be present behind the incident shock in the experiments is again ignored here for simplicity. The incident shock was placed at $z^* = 1$, using the analytical jump conditions for a Mach 1.47 shock in argon. (To minimize start-up transients, the initial shock jump was smeared over five grid points using an error-function profile.) Conditions are uniform for $z^* < 2$, except in the vicinity of the shock. The region $z^* > 2$ represents the plasma; the temperature profile is given by the heating model discussed above, and the pressure was taken as uniform.

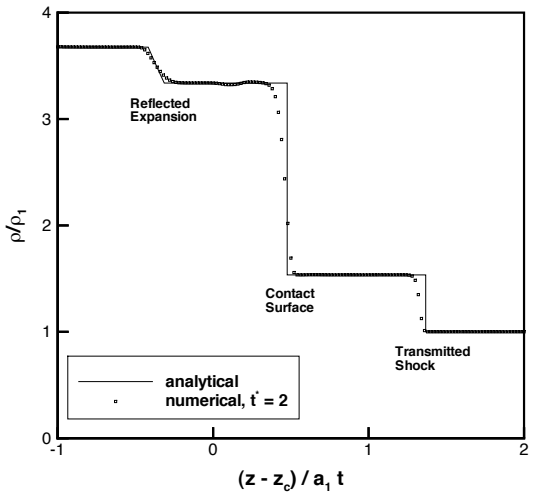

Fig. 7 Density profile through one-dimensional interaction of shock and contact surface (argon, $M_I = 1.47$, $T_5 = 300$ K, $T_1 = 659$ K).

A symmetry boundary condition was imposed on the centerline, and the radial velocity component was set to zero at the tube wall. Extrapolation was used at the left and right boundaries.

As a first check of the axisymmetric computation, a case was run for comparison with the one-dimensional analytical solution. The initial conditions were similar to those shown in Fig. 6, except that the region $z^* > 2$ was taken to have a uniform temperature of $T_1 = 659$ K, the centerline value predicted by the heating model for $I = 100$ mA. Figure 7 shows density profiles along the centerline ($r^* = 0$) for this case, plotted against the similarity variable $(z - z_c)/a_1 t$. The symbols represent the computed values for $t^* = 2$, and the solid lines are the analytical solution. The numerical model is seen to predict with good accuracy the positions (or equivalently the speeds) of the reflected expansion, the contact surface, and the transmitted shock. The detailed features of these structures are somewhat smeared by the numerical diffusion inherent in the computational technique.

Next, a grid resolution study was carried out in which the number of grid points was increased from $26 \times 5 \times 151$ to $51 \times 5 \times 301$, and the time step was decreased from $\Delta t^* = 1 \times 10^{-3}$ to $\Delta t^* = 5 \times 10^{-4}$. Figure 8 shows the pressure field for both cases at a stage shortly after the shock hits the contact surface. The upper part of the figure shows the results for the coarse grid computation, the lower part shows the results for the fine grid computation. The topology of the pressure fields in the two cases is identical, and the positions of the transmitted shock, the reflected expansion, and a pressure-maximum at the sidewall are essentially the same for the two plots. As expected, the smearing of the shock and expansion is reduced with

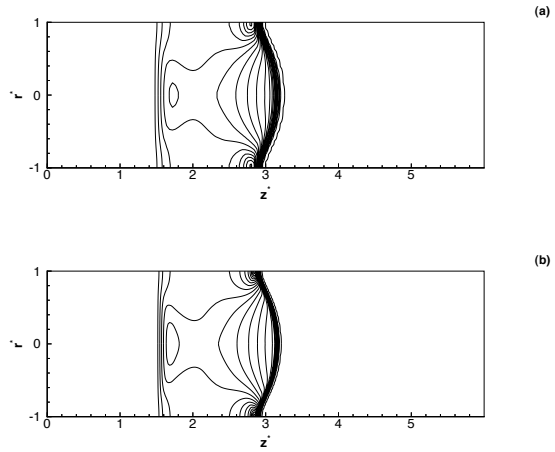

Fig. 8 Grid resolution study. 4 kPa argon for $t^* = 1.38$, $I = 163$ mA, $M_I = 1.3$, $\Delta p^* = 0.025$. (a) Coarse grid: $26 \times 5 \times 151$, $\Delta t^* = 1 \times 10^{-3}$. (b) Fine grid: $51 \times 5 \times 301$, $\Delta t^* = 5 \times 10^{-4}$.

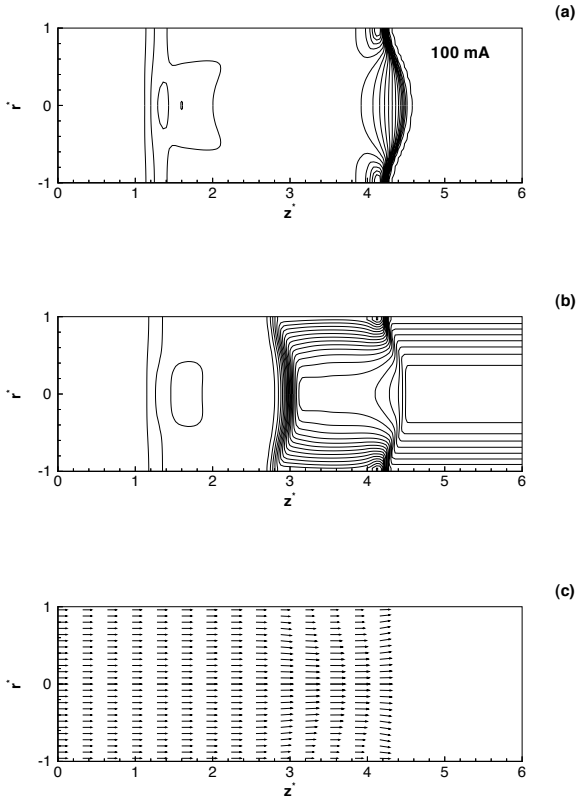

Fig. 9 Flowfield for $I = 100$ mA in 4 kPa argon at $t^* = 2$. (a) Pressure. (b) Density. (c) Velocity vectors.

grid refinement, and some small quantitative changes in the pressure field are observed.

Subsequent computations were carried out using the coarser grid resolution. Figure 9 shows the basic features of the flow for the 100 mA case at $t^* = 2$. The pressure field is shown in Fig. 9a, where the contour interval is $\Delta p^* = 0.05$. The bowed shock wave is ev-

ident in the vicinity of $z^* \approx 4.4$. Upstream of the shock (to the right), the pressure has a uniform value of $p = 4$ kPa. The shock is strongest in the vicinity of the wall, where a local maximum appears in the pressure field. Approaching the centerline from the wall along the downstream side of the shock, the pressure is seen to drop, then rise again toward the centerline. Relatively weak pressure variations are seen away from the shock, although the reflected expansion wave is detectable in the vicinity of $z^* \approx 1.2$.

The transmitted shock and reflected expansion wave are also visible in the density field (Fig. 9b), along with some additional features. The contour interval is $\Delta\rho^* = 0.05$, and the radial profile of density set by the heating model is evident upstream of the shock. A local maximum in the density is present near the wall, in the same location as the corresponding pressure maximum. In contrast to the pressure, the density on the downstream side of the shock drops monotonically from the wall toward the centerline. The contact surface lies near $z^* \approx 2.8$; like the shock it is bowed toward the right. A region of higher density is present to the left of the contact surface.

Figure 9c shows a relatively uniform velocity field. (Vectors for every eighth point in the z-direction, and every other point in the r-direction, are shown in the plot.) Between the contact surface and the shock the flow is faster near the centerline than near the walls, with a slight inflow toward the centerline. Close to the shock, however, the speed is more uniform, with slight flow away from the centerline. Note that the maxima in the pressure and density do not indicate flow separation; there is no recirculation present in the flowfield.

Since computations from previous studies of the spark-tube experiments were carried out for two-dimensional, planar symmetry rather than the more realistic two-dimensional, axial symmetry, a computation was carried out to examine the differences between the flows in the two configurations. The computation was carried out on a two-dimensional, Cartesian grid, designed to correspond to the case shown in Fig. 9. The same time step and grid resolution were used in the Cartesian case, along with analogous boundary conditions. In particular, the profile $T(r)$ for $I = 100$ mA was imposed as $T(y)$ in the Cartesian case.

Figure 10 compares the computations with planar (Fig. 10a) and axial (Fig. 10b) symmetry. As in the previous figure, the contour interval for the density field is $\Delta\rho^* = 0.05$. Although the qualitative features of the two flows are essentially the same, there is a substantial quantitative difference between the two cases. The shock bowing is about 40% greater in the planar case than in the axisymmetric case, and the corresponding shock speed is noticeably ($\sim 5\%$) greater.

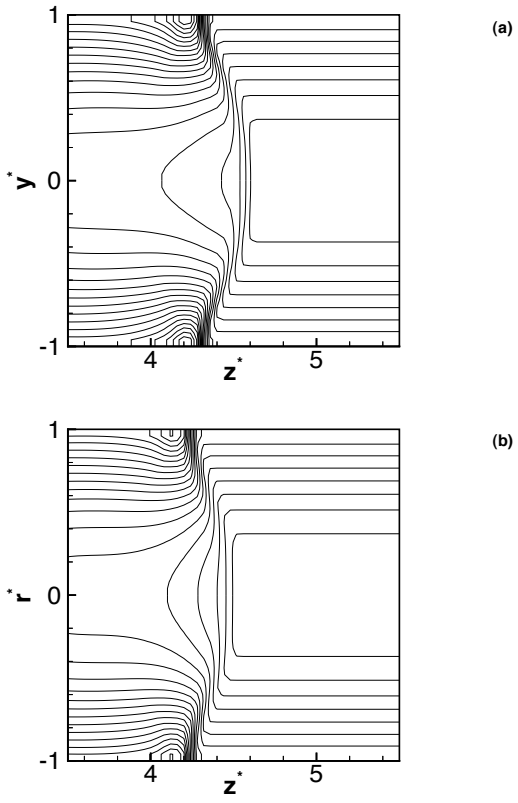

Fig. 10 Density field for $I = 100$ mA in 4 kPa argon at $t^* = 2$. (a) Two-dimensional, planar symmetry. (b) Two-dimensional, axial symmetry.

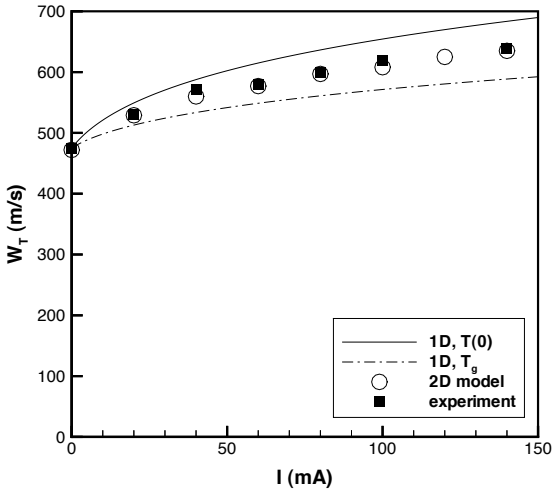

Fig. 11 Transmitted shock speed as a function of discharge current in argon at 4.0 kPa (30 torr).

Comparison with Experiment

For the set of experiments carried out in argon, the average shock-pulse velocity between the two photodetector stations was chosen as an unambiguous parameter for comparison to the theoretical models. The arrival time at each of the two stations was determined

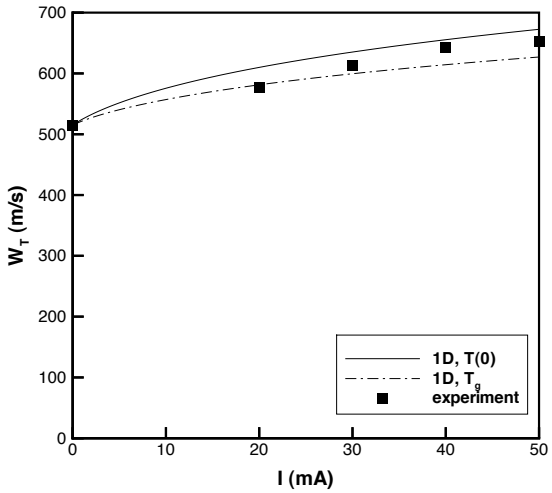

Fig. 12 Transmitted shock speed as a function of discharge current in nitrogen at 2.0 kPa (15 torr).

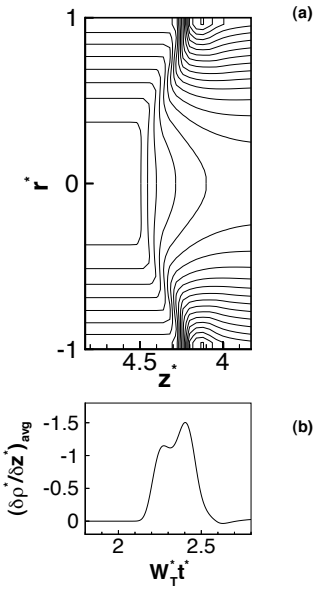

Fig. 13 Shock signature in photodetector signal, $I = 100$ mA in argon at 4 kPa. (a) Density field, $t^* = 2$. (b) Directional derivative along axis, averaged along radius, $z^* = 3$.

by the first rise above the ambient signal level discernible by eye in the time-series plots in Ganguly *et al.*[7] The average velocity of the shock pulse between the two stations was determined by dividing the distance between stations (120 mm) by the difference in arrival time.

Figure 11 shows the shock speed predicted for different current levels by both the one-dimensional and two-dimensional fluid models. The lines indicate the predictions of the one-dimensional model for two choices of the parameter T_1: the centerline temperature (solid line) and the average gas temperature (dash-dot line). The open symbols indicate values derived from the axisymmetric computation using the full temperature profile from the heating model. Both the one- and two-dimensional models are required to agree with the experiment for the zero-current case; there is no contact surface for this case because there is no axial temperature variation. The one-dimensional model is seen to provide a fair estimate of the trend predicted by the more realistic axisymmetric model; the predictions for the two choices of the parameter T_1 bracket the computational results.

The experimental average shock speeds are indicated by filled, square symbols in Fig. 11. The shock speed is seen to rise from an initial value of about 470 m/s with no current flowing to about 640 m/s at $I = 140$ mA. The predictions from the combination of the temperature profile from the heating model and the axisymmetric, inviscid-flow computation are seen to agree with the experiments within the scatter in the experimental data, and within the uncertainty in determining the shock speed from the computed flow field.

Figure 12 shows an analogous set of results for nitrogen. Here the distance between the measurement stations was 25.9 mm, and the data correspond to the set of detectors closer to the spark gap. As noted above, a good estimate of the parameter η was not available for this case. A value of $\eta = 0.2$ used with $E/N = 3 \times 10^{-20}$ V-m^2 in the model was found to give a good fit to the experimental data. Despite the use of an adjustable parameter in this case, it can be concluded that the data are again consistent with the trend predicted by the combination of the heating model and the one-dimensional flow model.

One interesting observation in the spark-tube experiments was the appearance of multiple peaks in the photodetector signal when the plasma was present. These peaks have been attributed to a splitting or dispersion of the shock.[7,8] A numerical simulation of the photodetector signal was carried out to investigate this phenomenon.

As the laser beam passes through the experimental apparatus, it is deflected by changes in index of refraction brought about by density variations. The slits in front of the photodetectors cut out a portion of the deflected beam, so that the amount of light reaching the photodetectors is a function of the beam deflection. The signal recorded by the photodetectors corresponds to the derivative of density along the direction normal to the slits (i.e., along the axis of the tube), averaged over the optical path.

Figure 13b shows a simulated laser deflectometer signal: the average across the radius of the directional derivative $\partial\rho^*/\partial z^*$ plotted against an effective distance $W_T^* t^*$. (The derivative was computed using a central difference.) For comparison, Fig. 13a shows a

portion of the density field; the z-axis has been flipped to correspond to the lower plot. The bowed shock is seen to produce a double-peak signal, as seen in the experiments. For this case (argon, 4kPa, 100 mA), the interval between the peaks corresponds to a distance of on the order of 3 mm or a time on the order of 5 μs. The total width of the pulse is roughly three times this scale.

The relationship between the flow non-uniformity and the double-peak in the photodetector signal was first explained by Bailey and Hilbun[3,9] in the context of their two-dimensional, planar computations. A qualitatively similar phenomenon is observed with the present, axisymmetric computations.

Conclusions

An analytical and computational study was carried out to assess the relative importance of thermal effects in the experiments of Ganguly *et al.*[7,8] on shock propagation in a glow discharge. Since measurements of the temperature field were not available, an analytical heating model was developed to relate the temperature field in the ionized gas to the discharge current. The temperatures predicted by the thermal model were used as the initial conditions for one-dimensional and axisymmetric inviscid-flow models of the shock propagation. The combined models predicted shock speed as a function of the discharge current. For reasonable estimates of the input parameters in the gas heating model, it was possible to obtain an excellent fit of the shock speeds predicted by the model to the experimental data. The axisymmetric model predicted the double-peak in the photodetector signal that was observed in the experiments.

Past numerical studies of this problem have used an unrealistic two-dimensional, planar symmetry.[3,9–11] The present work shows that these models are qualitatively correct, but tend to exaggerate the speed increase and bowing of the shock in the heated region. The reason for the qualitative agreement is that the flow is quasi-one-dimensional; the simple analytical model presented here gave a very reasonable estimate of the increase in shock speed in the heated region.

It is unequivocal that the experimental results are qualitatively consistent with thermal effects: the shock displays increased speed and reduced strength in the glow discharge. Quantitative agreement between thermal models and the experimental data remains debatable because of the lack of temperature measurements. In particular, the roles of the purge flow and of natural convection inside the discharge tube in setting the initial temperature profile have not been investigated. Finite difference heat-conduction computations (not presented here) show that radial variation in the thermal conductivity tends to soften the temperature profile, reducing the temperature gradient in regions of high temperature. Temperature variations in the axial direction are undoubtedly present in the experiment; a good model of the glow discharge would be required to simulate them realistically.

Given the importance of thermal effects, future experiments must map the temperature field in detail in order to demonstrate that electromagnetic effects can have a significant influence on shock propagation in a weakly-ionized plasma.

Acknowledgments

This project was sponsored by the Air Force Office of Scientific Research, and monitored by M. Jacobs and S. Walker. This work was also supported in part by a grant of High Performance Computing time from the Department of Defense Major Shared Resource Centers at The Army Corps of Engineers Waterways Experiment Station (CEWES) and The Naval Oceanographic Office (NAVO). The author is indebted to D. Gaitonde for help in carrying out the numerical computations, and to A. Creese for assistance in the preparation of this paper.

References

[1]Gurijanov, E. P. and Harsha, P. T., "AJAX: New Directions in Hypersonic Technology," AIAA Paper 96-4609, November 1996.

[2]Bain, W. L., editor, *Proceedings of the 1st Workshop on Weakly Ionized Gases*, Wright Laboratory Aero Propulsion and Power Directorate, Wright-Patterson AFB, OH, 1997, 2 vols.

[3]Hilbun, W. M., *Shock Waves in Nonequilibrium Gases and Plasmas*, Ph.D. thesis, Air Force Institute of Technology, Wright-Patterson AFB, OH, October 1997.

[4]Bain, W. L., editor, *Proceedings of the 2nd Workshop on Weakly Ionized Gases*, AIAA, Reston, VA, 1998.

[5]Adamovich, I. V., Subramaniam, V. V., Rich, J. W., and Macheret, S. O., "Phenomenological Analysis of Shock-Wave Propagation in Weakly Ionized Plasmas," *AIAA Journal*, Vol. 36, No. 5, 1998, pp. 816–822.

[6]Klimov, A. I., Koblov, A. N., Mishin, G. I., Serov, Y. L., and Yavor, I. P., "Shock Wave Propagation in a Glow Discharge," *Soviet Technical Physics Letters*, Vol. 8, No. 4, 1982, pp. 192–194.

[7]Ganguly, B. N., Bletzinger, P., and Garscadden, A., "Shock Wave Damping and Dispersion in Nonequilibrium Low Pressure Argon Plasmas," *Physics Letters A*, Vol. 230, 1997, pp. 218–222.

[8]Bletzinger, P. and Ganguly, B. N., "Local Acoustic Shock Velocity and Shock Structure Recovery Measurements in Glow Discharges," *Physics Letters A*, 1999, to appear.

[9]Bailey, W. F. and Hilbun, W. M., "Baseline of Thermal Effects on Shock Propagation in Glow Discharges," *Proceedings of the 1st Workshop on Weakly Ionized Gases*, edited by W. L. Bain, Vol. 2, Wright Laboratory Aero Propulsion and Power Directorate, Wright-Patterson AFB, OH, 1997, pp. GG–1 – GG–18.

[10]Kremeyer, K., Nazarenko, S., and Newell, A., "The Role of Vorticity in Shock Propagation through Inhomogeneous Media," AIAA Paper 99-0871, January 1999.

[11]Macheret, S. O., Martinelli, L., and Miles, R. B., "Shock Wave Propagation and Structure in Non-Uniform Gases and Plasmas," AIAA Paper 99-0598, January 1999.

[12]Poggie, J., "Modeling the Effects of Weak Ionization on Supersonic Flow and Shock Waves," AIAA Paper 99-0867, January 1999.

[13]Voinovich, P. A., Ershov, A. P., Ponomareva, S. E., and Shibkov, V. M., "Propagation of Weak Shock Waves in Plasma of Longitudinal Flow [sic] Discharge in Air," *High Temperature*, Vol. 29, No. 3, 1991, pp. 468–476.

[14]Anderson, J. D., *Modern Compressible Flow, with Historical Perspective*, McGraw-Hill, New York, 1982.

[15]Razier, Y. P., *Gas Discharge Physics*, Springer, Berlin, 1991.

[16]White, F. M., *Viscous Fluid Flow*, McGraw-Hill, New York, 1991.

[17]Weast, R. W., editor, *CRC Handbook of Chemistry and Physics*, CRC Press, Boca Raton, FL, 69th ed., 1988.

[18]Churchill, S. W. and Chu, H. H. S., "Correlating Equations for Laminar and Turbulent Free Convection from a Horizontal Cylinder," *International Journal of Heat and Mass Transfer*, Vol. 18, No. 9, 1975, pp. 1049–1053.

[19]White, F. M., *Heat Transfer*, Addison-Wesley, Reading, MA, 1984.

[20]Courant, R. and Friedrichs, K. O., *Supersonic Flow and Shock Waves*, Interscience, New York, 1948.

[21]Paterson, S., "The Reflection of a Plane Shock Wave at a Gaseous Interface," *The Proceedings of the Physical Society*, Vol. 61, No. 2, 1948, pp. 119–121.

[22]Glass, I. I. and Patterson, G. N., "A Theoretical and Experimental Study of Shock-Tube Flows," *Journal of the Aeronautical Sciences*, Vol. 22, No. 2, 1955, pp. 73–100.

[23]Ford, C. A. and Glass, I. I., "An Experimental Study of One-Dimensional Shock-Wave Refraction," *Journal of the Aeronautical Sciences*, Vol. 23, No. 2, 1956, pp. 189–191.

[24]Mirels, H., "Laminar Boundary Layer behind Shock Advancing into Stationary Fluid," NACA Technical Note 3401, National Advisory Committee for Aeronautics, March 1955.

[25]Hollyer, R. N., "Attenuation in the Shock Tube: I. Laminar Flow," *Journal of Applied Physics*, Vol. 27, No. 3, 1956, pp. 254–261.

[26]Duff, R. E., "Laminar Boundary Layer Development behind Shock Waves in Argon," *The Physics of Fluids*, Vol. 1, No. 6, 1958, pp. 546–547.

[27]Bradley, J. N., *Shock Waves in Chemistry and Physics*, J. Wiley, New York, 1962.